Downstream effects from contemporary wind turbine deployments

Pryor, S.C.; Barthelmie, R.J.; Hahmann, Andrea N.; Shepherd, T.J.; Volker, Patrick

Published in:
Journal of Physics: Conference Series

Link to article, DOI:
10.1088/1742-6596/1037/7/072010

Publication date:
2018

Document Version
Publisher's PDF, also known as Version of record

Downstream effects from contemporary wind turbine deployments

IOP Conf. Series: Journal of Physics: Conf. Series **1037** (2018) 072010 doi:10.1088/1742-6596/1037/7/072010

Downstream effects from contemporary wind turbine deployments

S.C. Pryor[1], R.J. Barthelmie[2], A. Hahmann[3], T.J. Shepherd[1], P.Volker[3]

[1]Department of Earth and Atmospheric Sciences, Cornell University, Ithaca, NY 14853
[2]Sibley School of Mechanical and Aerospace Engineering, Cornell University, Ithaca, NY 14853
[3]Wind Energy Department, Technical University of Denmark, DK-4000 Roskilde

sp2279@cornell.edu

Abstract. High-resolution regional simulations of the downstream effects of wind turbine arrays are presented. The simulations are conducted with the Weather Research and Forecasting (WRF) model using two different wind turbine parameterizations for a domain centered on the highest density of current wind turbine deployments in the contiguous US. The simulations use actual wind turbine geolocations and turbine specifications (e.g. power and thrust curves). Resulting analyses indicate that for both WT parameterizations impacts on temperature, specific humidity, precipitation, sensible and latent heat fluxes from current wind turbine deployments are statistically significant only in summer, are of very small magnitude, and are highly localized. It is also shown that use of the relatively recently developed new explicit wake parameterization (EWP) results in faster recovery of full array wakes. This in turn leads to smaller climate impacts and reduced array-array interactions, which at a system-wide scale lead to higher summertime capacity factors (2-6% higher) than those from the more commonly applied 'Fitch' parameterization. Our research implies that further expansion of wind turbine deployments can likely be realized without causing substantial downstream impacts on weather and climate, or array-array interactions of a magnitude that would yield substantial decreases in capacity factors.

1 Introduction and Motivation

Electricity from wind turbines (WT) currently supplies 6% of the U.S. national consumption, but is projected to exceed 20% by 2030. Achieving this target would require an approximate quadrupling of installed wind energy capacity leading to questions regarding:

1) Possible impacts on the regional climate. WT extract momentum and increase the turbulent kinetic energy (TKE) behind the rotor and thus alter the near-field atmospheric properties. Hence it has been suggested that large onshore WT arrays may cause substantial perturbations to near-surface temperature, specific humidity, atmosphere-surface exchange of heat, water and momentum and even precipitation regimes [1-3]. However, very few assessments have been conducted for climatologically relevant time periods using realistic representations of both the WT locations and their interaction with the atmospheric flow field.
2) How to optimize total electrical power generation across multiple WT arrays. As described above each individual WT within an array extracts momentum and increases the turbulence intensity

downstream. Hence the action of upwind WT arrays may substantially degrade the wind resource for arrays further downstream [2,3]. The reduction of wind speed within a large array and/or directly downwind of it is primarily dictated by a balance between the removal of momentum due to the drag imposed by the WT and the flux of momentum down the gradient of wind speed (from aloft and to a lesser extent laterally). The 'deep array wake effect' (i.e. low wind speeds and hence low electrical power production from WT located near the center of large arrays) and the downstream perturbation of wind speed is generally larger in offshore wind farms [4,5]. This is because the surface is smoother (leading to lower mechanical production of turbulence and hence ambient turbulence intensity), and the boundary layer depth is generally lower. Both factors reduce the rate of momentum transfer from aloft. Hence, the majority of previous research has focused on interactions between WT array arrays deployed offshore. However, the overwhelming majority of WT are deployed onshore [6], thus there also a need to quantify the downstream recovery of the whole wind farm wake from onshore WT arrays.

We quantify the impact of onshore WT arrays on local and downstream climate conditions and the propagation of whole array 'wakes' using paired continuous year-long simulations conducted for 2008 using the Weather Research and Forecasting model (WRF, v3.8.1). WRF is applied at convection-permitting resolution and using actual WT locations and specifications (hub-height (HH), rotor diameter, power and thrust curves) for a nested model domain centered on the state of Iowa (model domain is shown in Fig. 1). The simulations are thus centered on the state with highest current WT densities. As of the end of 2014 there were approx. 3,200 WT deployed in Iowa to give a total installed capacity of approx. 5.2 GW and an average installed capacity density of ~ 0.04 MW km^{-2}. The mean HH of these WT is 78 m (σ = 8 m) and the mean rated power is 1.6 MW.

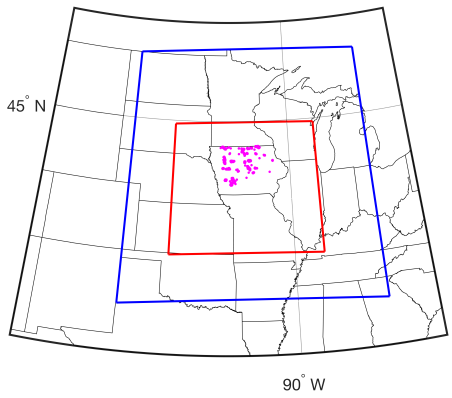

Fig. 1: Map of the central/eastern USA, with the simulation domains (d01 outlined in blue has a resolution of 12 km and d02 in red has 4 km resolution) and the locations of WT in Iowa as of the end of 2014 (magenta dots). The grey lines denote state boundaries. d01 comprises 149 by 149 grid cells, while d02 comprises 246 by 204 grid cells, 299 of which have WT within them. There are 41-layers in the vertical.

It is important to re-emphasize that the WT parameterization schemes applied herein are suitable for describing the 'far wake' (i.e. beyond a few rotor diameters). Our focus is on describing effects on the atmosphere at local to meso to regional scales (i.e. from a few kilometers to several hundred kilometers) deriving from a region of relatively high WT installed capacity.

Key innovations of this work include:

- The simulations employ actual WT locations, hub-heights and rotor diameters as of December 2014 (from https://eerscmap.usgs.gov/arcgis/rest/services/wind/wTurbinesWMDyn/MapServer) and rotor aerodynamics described using explicit WT power and thrust curves. Thus, our simulations use realistic WT densities and accurately represent the mechanisms by which they interact with the atmosphere.
- The duration of the simulations means it is possible to diagnose both the seasonality and diurnal cycle of any impacts on atmospheric properties downstream of WT arrays.
- Robust statistical metrics are used to characterize differences in near-surface temperature, specific humidity, wind speeds, precipitation and both sensible and latent fluxes.
- The discretization of the inner domain (4 km) is sufficient that it is 'convection resolving',

potentially leading to more accurate representation of, for example, the precipitation field [7].

An important aspect of our research is that we further seek to assess the degree to which the results differ dependent on the precise WT parameterization used within WRF. Use of two parameterized models of the WT rotor aerodynamics means we can sample an important component of the uncertainty space regarding the possible downstream impacts of WT, and enhance the robustness of resulting inferences.

2 Numerical Simulations

We conduct two sets of paired simulations for the nested domain shown in Fig. 1. The simulations are:
(a) A simulation without any wind turbines ('noWT1'), followed by an identical simulation using the Fitch wind farm parameterization [8] (defined as 'WT1').
(b) A simulation without any wind turbines ('noWT2'), followed by an identical simulation using the Explicit Wake Parameterisation, EWP [9] (defined as 'WT2').
The key difference between these two WT parameterizations is that while the Fitch scheme applies a (local) drag force and additional TKE to all model grid cells that intersect the turbine rotor, the EWP scheme parameterizes the unresolved wake expansion within the grid-cell and applies a grid-cell averaged drag force. In the EWP additional TKE results solely from enhanced vertical shear due to WT wake(s) and there is no addition of TKE directly from the WT [10].

In each pair of WRF simulations, all other settings are unchanged and for all simulations the lateral boundary conditions are supplied from the ERA-Interim reanalysis data [11]. The primary physics schemes applied are as follows:

- Longwave radiation: 1. Rapid radiative transfer model (RRTM) [12];
- Shortwave radiation: 1. Dudhia [13];
- Microphysics: 5. Eta (Ferrier) [14];
- Surface-layer physics: 1. MM5 similarity scheme [15];
- Land surface physics: 2. Noah land surface model [16];
- Planetary boundary layer: 5. Mellor-Yamada-Nakanishi-Niino 2.5 [17];
- Cumulus parameterization: Kain-Fritsch [18] is used in d01.

Three-dimensional fields of the wind components and 10-m wind speeds analyzed herein are output every 10-minutes, while all other parameters considered herein are output once hourly.

3 Results

Pairwise analyses of the noWT1 and WT1 output indicates that while the presence of WT changes wind speeds and near-surface air temperature (T2M) in 4 km grid cells in which WT are located (Fig. 2), the impact on T2M, specific humidity (Q2M), fluxes of latent and sensible heat, boundary layer heights and precipitation is not significant in any season other than summer. During summer, the maximum pairwise difference in grid cell mean T2M is 0.5 K (see Fig. 3) and the maximum increase in Q2M is 0.4 g kg^{-1} (Fig. 3). Quantile-quantile (QQ) plots (Fig. 2) illustrate that while the action of WT tends to increase the lowest T2M percentiles during winter (consistent with use of wind propellers in vineyards to prevent freezing), during summer they also slightly decrease the upper T2M percentiles. These effects are evident only in output from 4 km grid cells containing WT during winter, but there is also evidence of impacts on neighbouring grid cells in the summer (Fig. 2 and 3). Nevertheless, the impact of WT on the regional scale aggregate climate is small. The spatial average of the mean seasonal perturbation of T2M across the inner domain is < 0.1 K due to the presence of compensating positive and negative differences (the histograms of the grid-cell mean pairwise differences shown in Fig. 3 are almost symmetrical about zero). Precipitation probability is also not significantly impacted in any season other than summer. In the summer the presence of WT is associated with a small decrease in precipitation probability and a decrease in season total domain-wide precipitation of 2.6%. Differences of this magnitude are likely within the numerical uncertainty in the simulations and are smaller than could be detected in measurements.

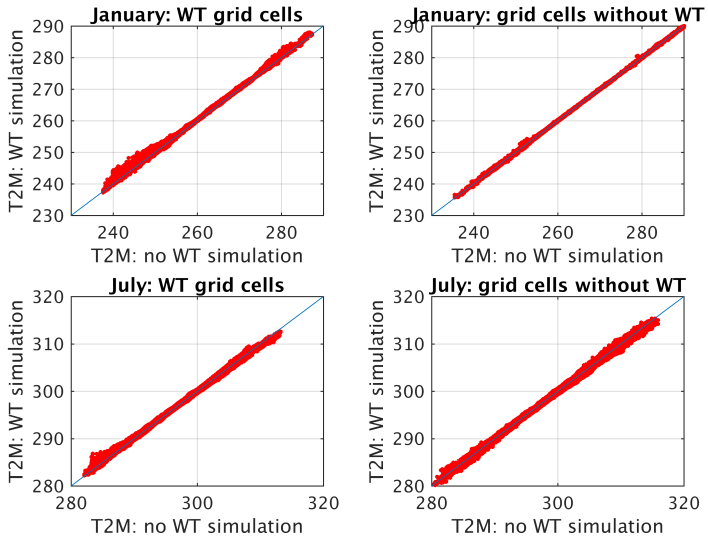

Fig. 2: Quantile-quantile plots of hourly air temperature at 2-m (T2M, in K) for (left) all of the 299 grid cells in d02 that contain WT during January and July and (right) 299 random grid cells without WT. The blue line corresponds to a 1:1 slope with zero intercept. The WT parameterization used is 'Fitch'.

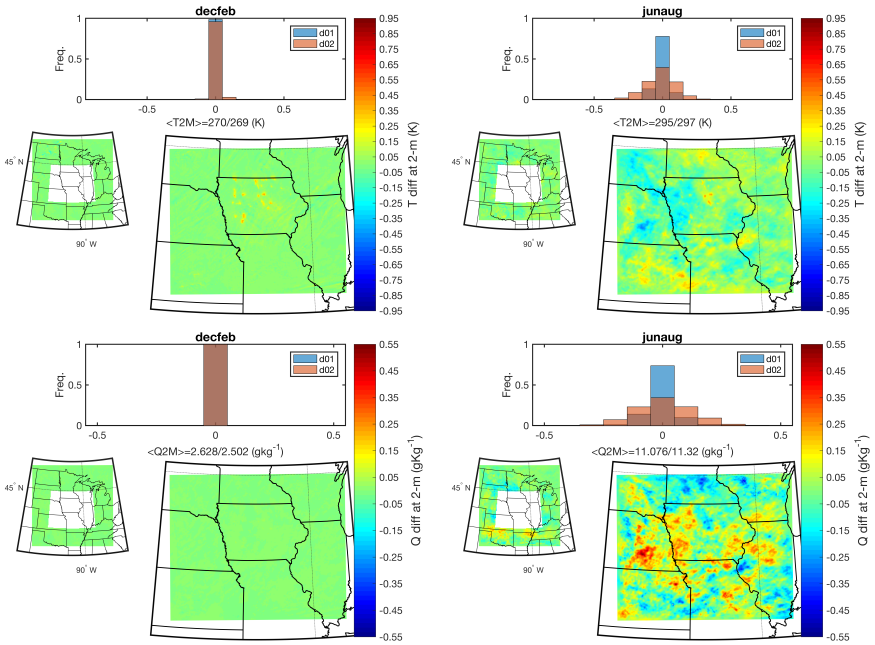

Fig. 3: Maps and histograms of the mean difference in each grid cell of (above) T2M and (below) specific humidity at 2-m (Q2M) in simulations with WT minus without WT (i.e. WT1 – noWT1) during winter (left) and summer (right). The values below the histograms denote the seasonal mean T2M and Q2M in d01 and d02 in the noWT1 simulation. The WT parameterization used is 'Fitch'.

Since summer is the only season in which notable WT impacts on near-surface temperature, specific humidity, sensible and latent heat fluxes and precipitation were observed in the WT1 versus noWT1 simulations, comparison of the two WT rotor aerodynamic parameterizations (Fitch v. EWP) described below focuses on the summer months only. Fig. 4 and 5 show spatial fields of the pairwise differences (WTX minus noWTX) in wind speed close to WT HH, and air temperature and specific humidity at 2-m from the Fitch parameterization and the EWP respectively for the months of June, July and August 2008. As is evident from these figures the perturbation to the wind speed field due to the presence of WT is generally more marked in the simulations using the Fitch parameterization (Fig. 4) than when EWP is applied (Fig. 5). Accordingly, the WT impacts on near-surface air temperature and specific humidity (along with the other parameters evaluated) are also typically more modest when the EWP parameterization is applied. Grid-cell mean differences in 2-m air temperature and specific humidity are generally symmetric about 0 in the pairwise evaluation of noWT1 and WT1, but results from the EWP simulation (i.e. WT2 minus noWT2) indicate that on average air temperatures are suppressed and specific humidity is increased by the action of the WT during the summer months.

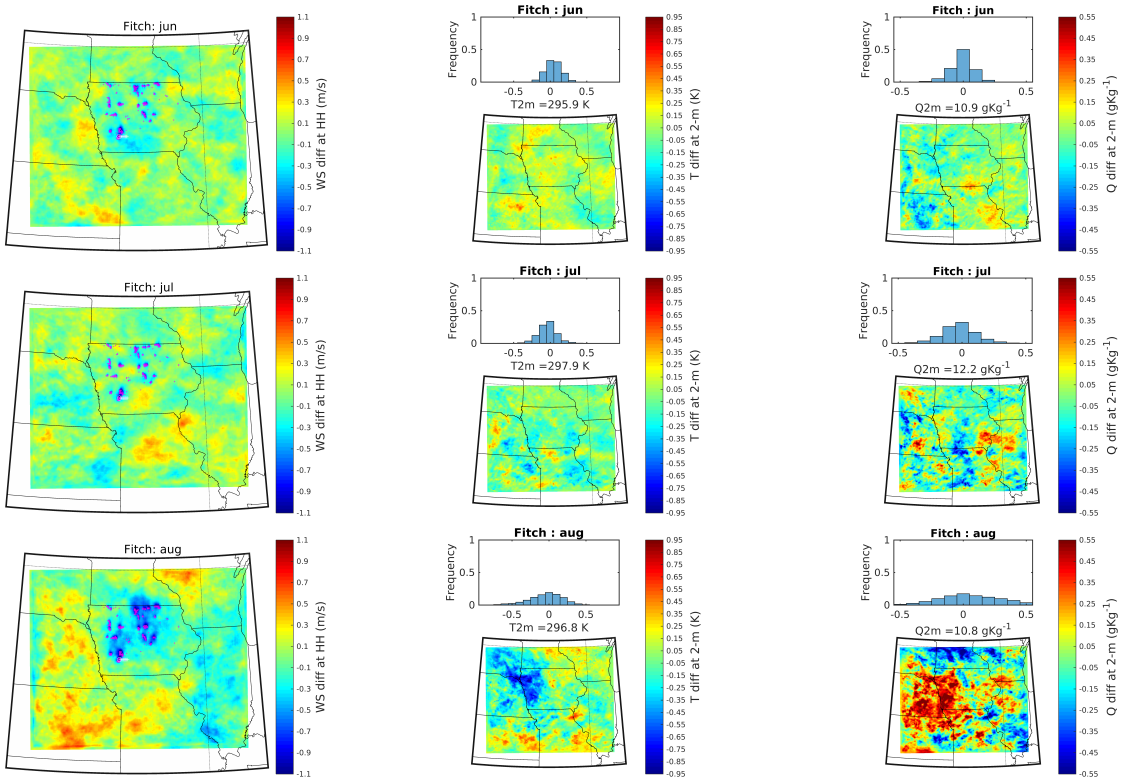

Fig. 4: Mean impact of WT on wind speed in the third model layer (WTHH, left), near-surface (2-m) air temperature (center) and near-surface (2-m) specific humidity (right) from WT1 minus noWT1 simulations for; June (top), July (middle) and August (bottom). Values below the histograms indicate mean d02 values from the noWT1 simulation.

Fig. 5 (below): As Fig. 4 but for WT2 minus noWT2.

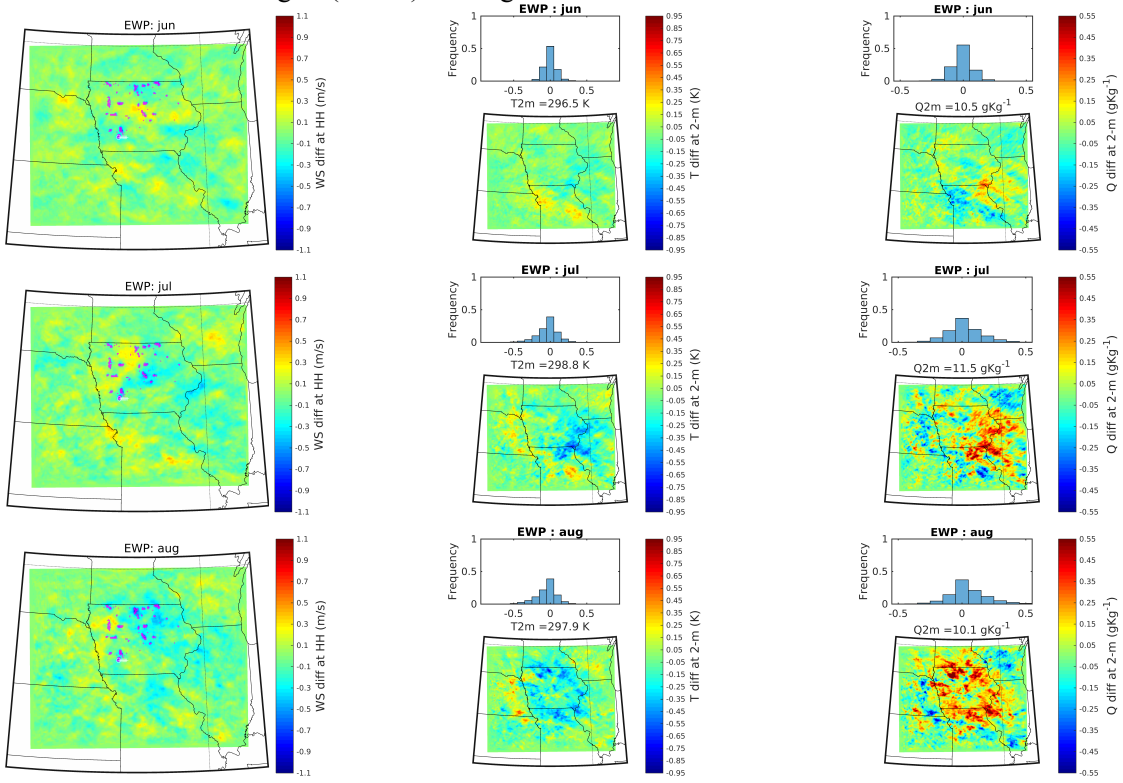

The WT1 simulations indicate realistic gross capacity factors in winter, spring, summer and fall of 52, 50, 33 and 48%, respectively. These are consistent with the high wind resource and thus relatively high wind penetration in the state of Iowa. Further, as indicated by these numbers, wind speeds are generally lower during the summer, but are frequently above cut-in wind speeds. Mean wind speeds from noWT1 over d02 at the model layer closest to the mean WT HH (i.e. layer-3) are; 11.5, 10.2 and 9.7 ms^{-1} in June, July and August, respectively. Hence, during summer WTs in Iowa experience wind speeds associated with relatively high wind turbine thrust coefficients and momentum extraction and thus generate comparatively intense wakes.

To provide a first assessment of the persistence and downwind propagation of 'whole wind farm wakes' from high-density WT arrays the following procedure is applied to the two sets of paired WRF simulations:

1) The 3×3 grid cell cluster with highest WT density (shown by the yellow circle in the spatial maps shown in the left panel of Fig. 6) is identified. This cluster is centred at approximately 41.24°N, 94.72°W, and the mean installed WT capacity within this 12 by 12 km area is ~ 2 MW km^{-2}.
2) Output from the paired simulations (noWT1 and WT1, and noWT2 and WT2) are conditionally sampled during each of the three summer months to select all 10-minute cases when in both sets of simulations flow over the grid cell directly west of this cluster is westerly (wind direction: 260-280°) and the 'freestream' wind speed in the third vertical level (approx. 83m, and thus close to the mean WT hub-height) exceeds 3 ms^{-1}. For the month of June 84 such cases are available for the simulations with the Fitch parameterization, while 92 such cases are available for the EWP simulations. The difference in sample size is due largely to a difference in the number of 10-minute periods during which the freestream wind speed in the grid cells containing this WT array exceeds the threshold of 3 ms^{-1}. For the other two months many fewer cases fulfil the selection criteria, thus in the following only the June cases are considered.
3) Output from the noWT1 simulation and the WT1 simulation and the noWT2 and WT2 simulations are extracted for the eight grid cells directly east of the 3×3 grid cluster (shown by the yellow + symbols in Fig. 6).
4) An approximation of the wake intensity is made by pairwise subtraction of the freestream wind speed (i.e. the wind speed from the third vertical layer in the grid cell upwind of the array) from the wind speed in each 'waked' (i.e. downwind) grid cell.
5) Boxplots and mean values of the wake intensity are developed for both of the noWTX and WTX simulations. In the noWTX simulation any wind speed difference in the freestream and downwind grid cells reflect only mesoscale meteorological effects such as those that would derive from topographic variability. While in the WTX simulation this wind speed difference is a function both of any terrain effects plus the wind farm wake. As shown in Fig. 6, for the first four downwind grid cells the mean wind speed difference in the noWT1 simulation is zero, beyond that distance there is evidence of higher wind speeds (of upto 1 ms^{-1} above than the freestream on average) with increasing distance east. This is consistent with a decrease in terrain elevation of approx. 50 m. The WT1 simulation exhibits evidence of a whole wind farm wake, with mean wind speeds that are approximately 0.8 ms^{-1} lower than the freestream in the two grid cells immediately downwind of the high-density array (Fig. 6).
6) The downwind distance at which the wind farm wake has dissipated is diagnosed in two ways:
    i. Firstly, as the downwind distance at which the median values of the 'wake intensity' from noWT1 and WT1 (or noWT2 and WT2) are equal.
    ii. Secondly, as the downwind distance at which the mean wake deficit in the WT1 or WT2 simulation is 0.

As shown in Fig. 6, in the noWT1 and WT1 simulations using these two approaches the wind farm wake from this high-density large WT array is no longer detectable at 16 km (i.e. 4 grid cells) and 20 km (i.e. 5 grid cells) downstream, respectively. The differences in wind speeds from noWT1 and WT1

manifest at greater downwind distances (Fig. 6) appear to derive from the advection of wakes from other upwind WT arrays (most notably to the northwest). When the same procedure is applied to noWT2 and WT2 simulation output the results indicate the wake from this high-density large WT array is no longer detectable using both approaches at 16 km (i.e. 4 grid cells) downstream. Thus there is some evidence that the downstream propagation of the velocity deficit from large arrays is greater for the Fitch parameterization than the EWP. This is consistent with previous research for a theoretical very large onshore wind farm (i.e. > 1×10^5 km^2 area covered by over 160,000 WT placed with a 10.5 rotor diameter spacing) that found the distance downstream from the edge of the wind farm at which the asymptotic wind speed at hub-height is reached is 30 km in simulations with the Fitch scheme, but is only 17 km downstream in the EWP [19].

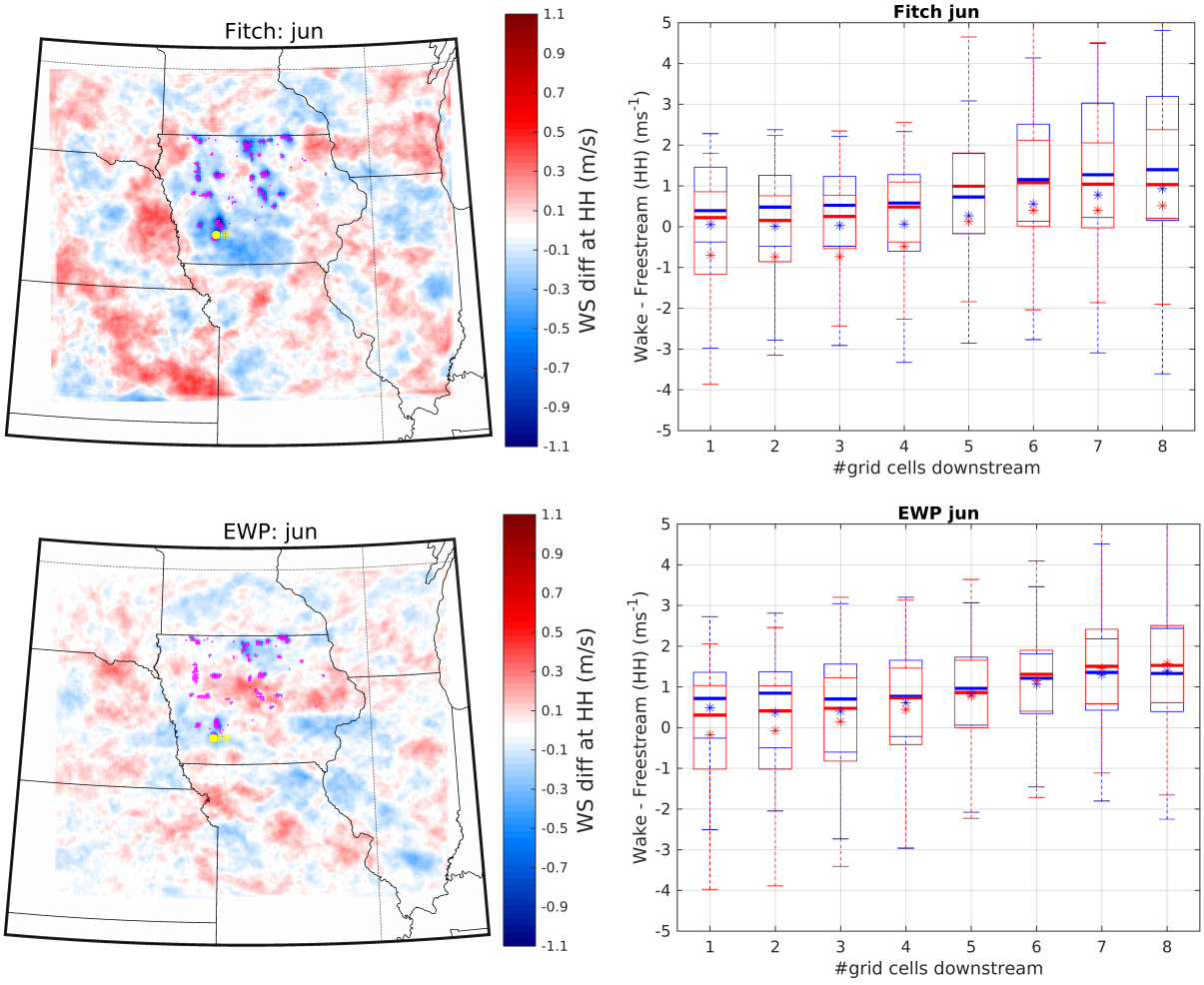

Fig. 6. Left: A map of the mean pairwise difference in wind speeds within d02 from the third model layer (~ 83 m) in the WT1 minus noWT1 simulations (above) and the WT2 minus noWT2 simulations (below) for climate conditions as prevailed during the month of June 2008. The magenta dots indicate the locations of WT. The yellow circle denotes the center of the 3×3 grid cell cluster with the highest total WT installed capacity, while the yellow + symbols denote the 8 downwind grid cells used in the whole wind farm wake assessment summarized in the right-hand panel. Right: Boxplots of the difference in freestream wind speed in the third model layer subtracted from the wind speed in the downwind grid cells. The mean value is denoted by the *, while the thick horizontal line shows the median. For both the Fitch and EWP WT parameterizations the boxplots shown in blue indicate the noWTX simulation, while those shown in red depict the WTX simulation.

To quantify the impact of the WT parameterization on the total system performance, system-wide capacity factors are computed. Differences in the wake behaviour between the two simulations have a substantial impact on the total power production from WT deployed in Iowa (Fig. 7 and Table 1). The shorter recovery distance for onshore wind turbine arrays derived using the EWP scheme substantially reduces the amount of 'wind theft' experienced by downwind WT arrays and thus generates higher system-wide electrical power production. Accordingly, the empirical cumulative probability plot for differences in each 10-minute period show that while some 10-minute periods exhibit lower electrical power production in the simulation using the EWP description, the large majority exhibit higher power production (Fig. 7) leading to higher monthly system-wide capacity factors in the simulations with EWP (Table 1). These findings should not be taken as evidence that one WT wake parameterization is superior to the other, but rather that array-array interactions and also the downstream inadvertent modification of meteorological conditions exhibits a sensitivity to the WT parameterization employed within WRF.

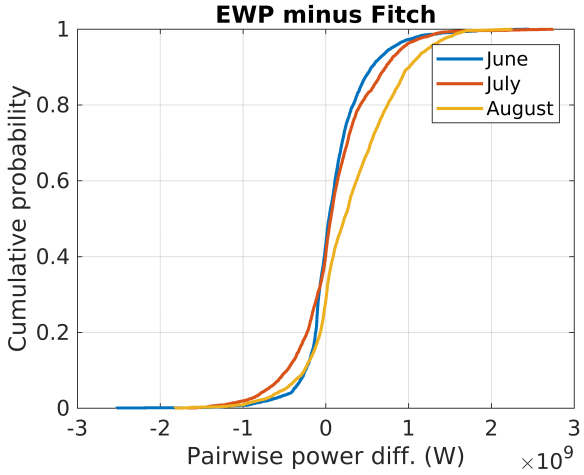

Fig. 7: Empirical cumulative probability plots of the pairwise differences in all 10-minute total power production estimates from all WT in Iowa for the three summer months of 2008. The differences are computed for all 10-minute periods in each month as the difference in domain-wide total power in simulations with EWP minus those from Fitch (i.e. WT2-WT1).

Table 1. Domain-wide capacity factors for WT in Iowa for the three summer months of 2008 computed using simulations employing the Fitch (WT1) and EWP (WT2) WT parameterizations within WRF.

Month	Capacity factor in simulations with Fitch parameterization (WT1)	Capacity factor in simulations with EWP parameterization (WT2)
June	38	40
July	30	32
August	30	36

4 Conclusions and Implications

Our research has evolved two key findings:

1. Simulated climate impacts from WT deployments are of very modest magnitude and are maximized in summer due to the lower wind speeds during this season and WT aerodynamics. Our finding of only modest impacts on regional climate from WT deployed at current and near-term (next 20-year) densities are consistent with results from coarser spatial resolution simulations over Europe [1]. These results also indicate that previous studies based on shorter duration summertime simulations from very high-density WT arrays in the US Central Plains [2,3] may not be representative of the long term climate impacts from WT deployments.
2. Inadvertent flow and climate modification from WT arrays exhibits a substantial dependence on the description of the WT rotor aerodynamics (i.e. the WT parameterization employed in the WRF simulations). The EWP approach tends to lead to WT array wakes that dissipate more rapidly in the atmosphere and thus lead to both smaller scale impacts on near-surface climate variables and

smaller array-array interactions. This latter effect leads to a substantial difference in the overall capacity factors computed for WT deployed in the state of Iowa, with EWP indicating state-wide capacity factors that are 2-6% higher in the summer months than those computed in simulations using the Fitch parameterization.

It may be that the very modest impacts on the local to mesoscale and regional climate generated for both WT wake parameterizations are due in part to our use of a sufficiently highly resolved inner domain (d02) that a cumulus parameterization is not required and further that the model resolution applied may play a role in determining the seasonality of WT impacts. In this latter context it is important to note that the added value of convection permitting model simulations "potentially exists where/when deep convection is a dominant process (e.g., tropics, subtropics, and midlatitude summer)" [7]. The high resolution of the simulations presented herein, may also impact the wake recovery distances reported herein, as does the precise approach used to define the point at which the wind farm wake is no longer detectable.

Eld is noFuture work should address the degree to which our findings are dependent on the resolution at which WRF is applied. Additional sources of uncertainty that could be addressed in future work include:

(a) The dependence of differences between the two WT parameterizations on the simulated wind regime. The study domain exhibits pronounced inter-annual variability in wind speeds in part due to major climate modes such as the El Niño-Southern Oscillation [20,21].

(b) The sensitivity of results to the precise description of WT wakes in the two parameterizations (e.g. the length scale that determines the rate of WT wake expansion within the EWP), and to the definition used to quantify the downstream distance at which the whole-wind farm wakes are no longer detectable.

5 Acknowledgments

The US Department of Energy (DE-SC0016438) and Cornell University's Atkinson Center for a Sustainable Future (ACSF-sp2279-2016) funded this research. We thank Adam Brazier, Brandon Barker and Bennett Wineholt for their assistance in building and maintaining the cloud infrastructure leveraged in this research. This research was enabled by access to a range of computational resources supported by NSF; ACI-1541215, those made available via the NSF Extreme Science and Engineering Discovery Environment (XSEDE) (award TG-ATM170024), and those of the National Energy Research Scientific Computing Center, a DOE Office of Science User Facility supported by the Office of Science of the U.S. Department of Energy under Contract No. DE-AC02-05CH11231.

6 References

[1] Vautard, R. *et al*. 2014. Regional climate model simulations indicate limited climatic impacts by operational and planned European wind farms. *Nature Communications* **5**, doi: 10.1038/ncomms4196.

[2] Baidya Roy, S., Pacala, S. W. & Walko, R. L. 2004. Can large wind farms affect local meteorology? *Journal of Geophysical Research* **109**, D19101, doi:19110.11029/12004JD004763.

[3] Miller, L. M. *et al*. 2015. Two methods for estimating limits to large-scale wind power generation. *Proceedings of the National Academy of Sciences* **112**, 11169-11174, doi:10.1073/pnas.1408251112.

[4] Barthelmie, R. J. *et al*. 2009. Modelling and measuring flow and wind turbine wakes in large wind farms offshore. *Wind Energy* **12**, 431-444. DOI: 410.1002/we.1348.

[5] Barthelmie, R. J., Hansen, K. S. & Pryor, S. C. 2013. Meteorological controls on wind turbine wakes. *Proceedings of the IEEE* **101(4)**, 1010-1019.

[6] Wiser, R. *et al*. 2016. Expert elicitation survey on future wind energy costs. *Nature Energy* **1**, 16135, doi:10.1038/nenergy.2016.135.

[7] Prein, A. F. *et al*. 2015. A review on regional convection-permitting climate modeling:

Demonstrations, prospects, and challenges. *Reviews of Geophysics* **53**, 323-361.

[8] Fitch, A. C., Olson, J. B. & Lundquist, J. K. 2013. Parameterization of Wind Farms in Climate Models. *Journal of Climate* **26**, 6439-6458, doi:10.1175/jcli-d-12-00376.1.

[9] Volker, P. J. H., Badger, J., Hahmann, A. N. & Ott, S. 2015. The Explicit Wake Parametrisation V1.0: a wind farm parametrisation in the mesoscale model WRF. *Geoscientific Model Development* **8**, 3481-3522. doi:3410.5194/gmdd-3488-3481-2015.

[10] Barthelmie, R. J. *et al*. 2007. Modelling and measurements of power losses and turbulence intensity in wind turbine wakes at Middelgrunden offshore wind farm. *Wind Energy* **10**, 217-228.

[11] Dee, D. P. *et al*. 2011. The ERA-Interim reanalysis: Configuration and performance of the data assimilation system. *Quarterly Journal of the Royal Meteorological Society* **137**, 553-597.

[12] Mlawer, E. J., Taubman, S. J., Brown, P. D., Iacono, M. J. & Clough, S. A. 1997. Radiative transfer for inhomogeneous atmospheres: RRTM, a validated correlated-k model for the longwave. *Journal of Geophysical Research: Atmospheres* **102**, 16663-16682.

[13] Dudhia, J. 1989. Numerical study of convection observed during the winter monsoon experiment using a mesoscale two-dimensional model. *Journal of the Atmospheric Sciences* **46**, 3077-3107.

[14] Ferrier, B. S. *et al*. 2002. Implementation of a new grid-scale cloud and precipitation scheme in the NCEP Eta model. *15th Conf. on Numerical Weather Prediction*, 280-283.

[15] Beljaars, A. 1995. The parametrization of surface fluxes in large-scale models under free convection. *Quarterly Journal of the Royal Meteorological Society* **121**, 255-270.

[16] Tewari, M. *et al*. 2004. Implementation and verification of the unified NOAH land surface model in the WRF model. *20th Conference on Weather Analysis and Forecasting/16th Conference on Numerical Weather Prediction* **1115**, 6pp.

[17] Nakanishi, M. & Niino, H. 2006. An improved Mellor–Yamada level-3 model: Its numerical stability and application to a regional prediction of advection fog. *Boundary-Layer Meteorology* **119**, 397-407.

[18] Kain, J. S. 2004. The Kain–Fritsch convective parameterization: an update. *Journal of Applied Meteorology* **43**, 170-181.

[19] Volker, P. J. H., Hahmann, A. N., Badger, J. & Jørgensen, H. E. 2017. Prospects for generating electricity by large onshore and offshore wind farms. *Environmental Research Letters* **12**, 034022.

[20] Pryor, S. C. & Ledolter, J. 2010. Addendum to: Wind speed trends over the contiguous USA. *Journal of Geophysical Research* **115, D10103**, 10.1029/2009JD013281.

[21] Schoof, J. T. & Pryor, S. C. 2014. Assessing the fidelity of AOGCM-simulated relationships between large-scale modes of climate variability and wind speeds. *Journal of Geophysical Research: Atmospheres* **119**, 9719-9734.